Design of "model-friendly" turbulent non-premixed jet burners for C2+ hydrocarbon fuels

Jiayao Zhang, Christopher R. Shaddix, and Robert W. Schefer

Articles you may be interested in

Comparative analysis of low- and high-swirl confined flames and jets by proper orthogonal and dynamic mode decompositions
Phys. Fluids **26**, 065109 (2014); 10.1063/1.4884915

An automated thermophoretic soot sampling device for laboratory-scale high-pressure flames
Rev. Sci. Instrum. **85**, 045103 (2014); 10.1063/1.4868970

Investigations on the local entrainment velocity in a turbulent jet
Phys. Fluids **24**, 105110 (2012); 10.1063/1.4761837

Flashback of laminar premixed flame in rotating burner
AIP Conf. Proc. **1440**, 1292 (2012); 10.1063/1.4704350

Structure analysis of turbulent mixing patterns in inert and reactive turbulent liquid flows
Chaos **12**, 395 (2002); 10.1063/1.1478080

Design of "model-friendly" turbulent non-premixed jet burners for C$_{2+}$ hydrocarbon fuels

Jiayao Zhang, Christopher R. Shaddix, and Robert W. Schefer
Combustion Research Facility, Sandia National Laboratories, 7011 East Avenue, Livermore, California 94550, USA

Experimental measurements in laboratory-scale turbulent burners with well-controlled boundary and flow configurations can provide valuable data for validating models of turbulence-chemistry interactions applicable to the design and analysis of practical combustors. This paper reports on the design of two canonical nonpremixed turbulent jet burners for use with undiluted gaseous and liquid hydrocarbon fuels, respectively. Previous burners of this type have only been developed for fuels composed of H$_2$, CO, and/or methane, often with substantial dilution. While both new burners are composed of concentric tubes with annular pilot flames, the liquid-fuel burner has an additional fuel vaporization step and an electrically heated fuel vapor delivery system. The performance of these burners is demonstrated by interrogating four ethylene flames and one flame fueled by a simple JP-8 surrogate. Through visual observation, it is found that the visible flame lengths show good agreement with standard empirical correlations. Rayleigh line imaging demonstrates that the pilot flame provides a spatially homogeneous flow of hot products along the edge of the fuel jet. Planar imaging of OH laser-induced fluorescence reveals a lack of local flame extinction in the high-strain near-burner region for fuel jet Reynolds numbers (*Re*) less than 20 000, and increasingly common extinction events for higher jet velocities. Planar imaging of soot laser-induced incandescence shows that the soot layers in these flames are relatively thin and are entrained into vortical flow structures in fuel-rich regions inside of the flame sheet. © *2011 American Institute of Physics*. [doi:10.1063/1.3605491]

I. INTRODUCTION

Laboratory-scale turbulent burners have been routinely used to study the fundamentals of non-premixed turbulent combustion. In fact, this type of burner has been a workhorse to advance the understanding of turbulent combustion and to improve combustion modeling, particularly through the activities of the International Workshops on Measurement and Computation of Turbulent Nonpremixed Flames (generally referred to as the "TNF Workshops").[1] Simple jet burners have the advantage of easily characterized inlet flow conditions and can be applied as open flames, facilitating the implementation of laser diagnostic experimental measurements and eliminating both experimental and computational complications arising from bound flows. As compared to simple jet burners,[2–4] piloted burners, utilizing a premixed "pilot" flame system that surrounds the fuel jet, can sustain stable flames burning a wide variety of fuels and at high jet velocity without experiencing liftoff or blowout. The most well-studied piloted combustor is the "Sydney burner,"[5] which has been the subject of extensive experimental[6–9] and computational[10–12] investigations. A similar burner is the Delft natural gas burner.[13] Other burners used as model combustors for studying turbulent combustion include the bluff-body combustor[14] and the TECFLAM swirl burner.[15] Designed for their own purposes, these latter two burners add complexity to the flow field and thus provide a more practical combustion environment. However, these burners are either complex in construction or have limited access for optical measurements.

In this paper, we describe the design of two non-premixed jet burners: one for C$_{2+}$ *gaseous* hydrocarbon fuels and the other for higher-C-number, *liquid* hydrocarbon fuels. Experimental studies of higher-C flames on these new burners allow the continuation of a natural progression from simple to complex fuel chemistry. There have been a number of previous experimental investigations of non-premixed turbulent jet flames of heavier hydrocarbon fuels, notably the acetylene flame studies of Magnussen and co-workers,[16,17] ethane, ethylene, propane, and acetylene flame studies by Becker and co-workers,[18–21] propane flame studies by Nishida and Mukohara,[22] acetylene and ethylene flame studies by Kent and co-workers,[23,24] propane, ethylene and acetylene flame studies by Faeth, Gore, and co-workers,[25–29] ethylene flames by Flower,[30] propane and ethylene flame studies by Turns and co-workers,[31–35] ethylene and kerosene flames by Young *et al.*,[36,37] and ethylene flames by Koylu and co-workers.[38,39] However, the burners employed in these previous studies were not expressly designed with modeling in mind and suffer from one or more important deficiencies in this regard, such as not providing a conditioned coflow of air, having insufficient fuel tube length to ensure a fully developed turbulent pipe flow profile at the nozzle exit, or having a poorly characterized pilot flame exit flow (in terms of velocity and temperature profile). Previous research has shown that these are important considerations in designing burners and conducting experiments that allow rigorous comparisons with models.[1,5,40]

The use of a pilot flame at the burner exit is not always required, particularly for fast-reacting fuels such as hydrogen and syngas. However, for hydrocarbon fuels, operation of a jet flame burner at a high enough flow velocity to create fully turbulent flow conditions generally results in a lifted flame (and

82, 074101-1

eventually flame blowoff) in the absence of a pilot flame to anchor the main jet flame. Köhler *et al.*[41] recently reported soot measurements made on an ethylene jet flame with a Reynolds number of 10 000 that was stabilized on an unpiloted burner. The lack of a pilot flame simplifies specification of the flow and temperature boundary condition at the burner exit plane, but, as shown by Köhler *et al.*, results in a lifted flame, even at a relatively low fuel jet Reynolds number. The presence of a lifted flame minimizes heat transfer back to the burner tube and uncertainty in the true fuel jet exit temperature. However, the flame liftoff height plays an essential role in the extent of fuel partial premixing that occurs and therefore must be accurately modeled to give meaningful downstream predictions. Furthermore, the complexity of the flame stabilization mechanism in lifted turbulent jets presents a challenge to modeling.[42]

With the use of heavier, undiluted hydrocarbon fuels, the formation of polycyclic aromatic hydrocarbons (PAH) and soot increases dramatically in non-premixed flames, particularly for practical liquid transportation fuels that contain aromatic species.[43] Soot and PAH pose a challenge to the detailed experimental study of these flames with typical laser diagnostic techniques such as Rayleigh scattering, Raman scattering, and laser-induced fluorescence (LIF).[1,44,45] Similarly, accurate modeling of the formation and destruction of PAH and soot in turbulent flames is currently a severe challenge, in and of itself.[46–49] For this reason, we have chosen to implement piloted burners and focus on intermediate values of fuel jet Reynolds numbers that do not suffer from substantial local extinction, which is challenging to model with even simple, well-understood fuel chemistry.[50–52] Five flames, using two different fuels, have been chosen as standard flames on these two new burners. Results from preliminary characterization of these flames with visual observation and optical diagnostics are reported here, demonstrating the favorable operational characteristics of the burner design.

II. DESIGN OF COMBUSTORS

This section introduces two piloted non-premixed jet burners used for gaseous and liquid fuels, respectively. The design fuel for the gas burner is pure ethylene, whereas that for the liquid burner is a mixture of *m*-xylene and *n*-dodecane (23:77 by liquid volume), which mimics the liquid density, H/C ratio, and sooting propensity of JP-8,[53] an aviation fuel used for military aircraft. While pure fuels have been used in our experiments conducted to-date, the fuel supply lines allow for fuel dilution, for instance, with nitrogen or air.

A. Gas fuel combustor

The gas burner is similar in design to the Sydney burner,[5] which has proven to be conducive to turbulent flame modeling.[10–12] As shown in Fig. 1, the burner consists of two concentric tubes, the inner one supplying a high-speed flow of the main fuel and the outer one delivering a low-speed pilot gas mixture. A plate with judiciously designed holes sits in the annulus between the two tubes and near the tube lips,
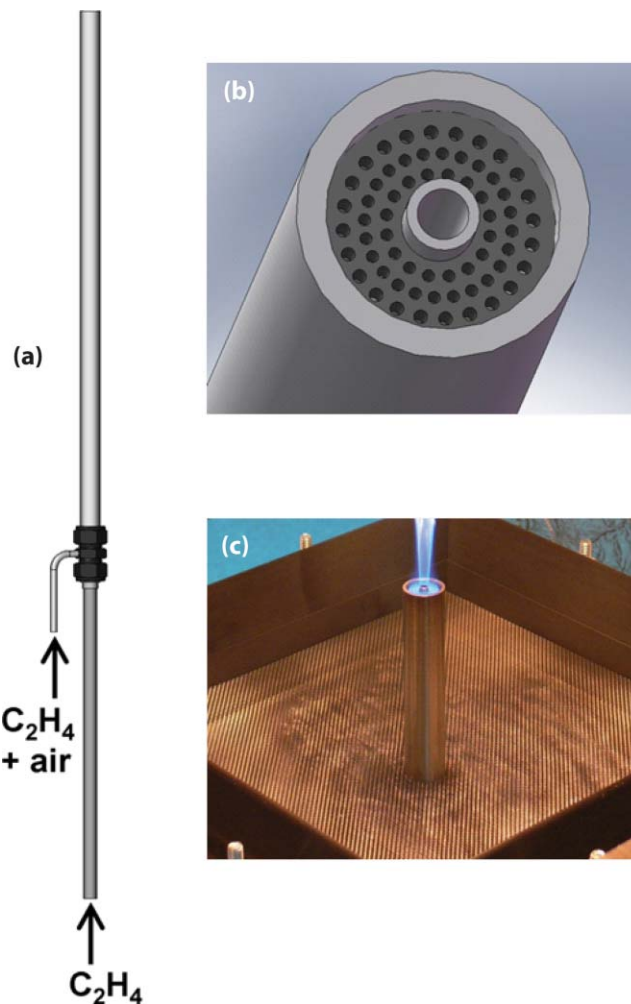

FIG. 1. (Color online) The piloted jet burner used for gaseous fuels: (a) drawing of the burner, with the central fuel tube supplying the fuel and the outer coannular tube supplying a premixed fuel-air mixture to an array of small pilot flames; (b) close-up view of the burner exit, showing the fuel tube surrounded by a perforated pilot plate; (c) base of a burning ethylene flame, with pilot flames appearing as small blue cones surrounding the main jet.

serving as an anchor for pilot flames. The flow rate of the pilot mixture corresponds to 2% of the heat release rate of the main jet, so as to minimize aerodynamic and thermal effects on the main flame while providing a stable ignition source.

When sizing the inner fuel tube, one is bound by several constraints. First, the flame height should be short enough that the vertical translation stage on which the burner resides can move the entire flame through the fixed optical probe volume. The maximum range of vertical translation is about 900 mm, setting the upper limit on the flame length. Second, frequent local extinctions should be avoided, since modeling of extinction and reignition chemistry would otherwise be required, which many combustion models cannot handle. Last, in order to study flames with sufficiently intense turbulence to be valuable to turbulent flame modelers,[1] the flame Reynolds number is targeted to be in the vicinity of 20 000, where the cold-jet Reynolds number is defined as $Re = \rho U_J D / \mu$, with U_J equal to the jet exit velocity, D the jet diameter, and ρ and μ the density and dynamic viscosity of the fuel at the burner exit.
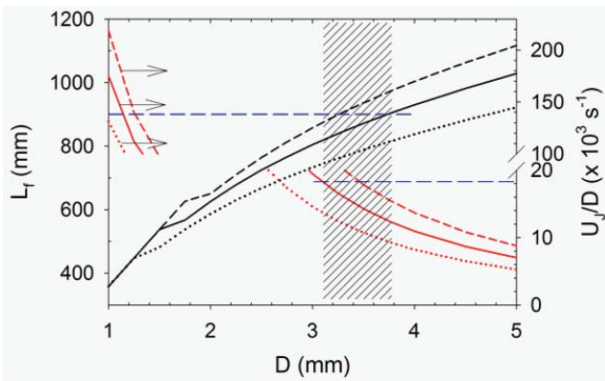
FIG. 2. (Color online) Estimated flame heights (left axis) and U_J/D (right axis) for ethylene as a function of fuel jet diameter. The flame height is required to be less than 900 mm, and U_J/D to be less than $1.8 \times 10^4 \, \mathrm{s}^{-1}$. Three Reynolds numbers are drawn: 20 000 (solid), 15 000 (dotted), and 25 000 (dash). The shadowed region identifies the allowable range of jet diameter when $Re = 20\,000$.

The flame height of our piloted non-premixed jet flames is estimated using the relation given in Refs. 54 and 55.

$$L_f = \begin{cases} \dfrac{13.5 Fr_f^{2/5}}{\left(1+0.07 Fr_f^2\right)^{1/5}} \cdot d_J^*/Z_{ST} & \text{for} \quad Fr_f < 5 \\[2mm] 23 d_J^*/Z_{ST} & \text{for} \quad Fr_f \geq 5 \end{cases}. \quad (1)$$

Fr_f is the flame Froude number, d_J^* the moment diameter, and Z_{ST} the stoichiometric mixture fraction; Further explanation can be found in Ref. 55. This relation, developed from simple jet flames, should also apply to our piloted jet flames, since the relatively small heat release and momentum of the pilot flame is not expected to alter the hydrodynamic and thermal structures of the main jet. Figure 2 shows the estimated ethylene flame length for $Re = 15\,000$, 20 000, and 25 000.

The occurrence of local extinction correlates with the global strain rate of the flow: the higher the strain rate, the more likely local extinction events will occur, ultimately leading to flame liftoff and then blowout. Strain rate is hard to quantify in jets, as it varies with location. Nevertheless, a rough scaling relation for strain rate, S, may be evaluated as,

$$S \sim \frac{U_C}{\delta_{\mathrm{FWHM}}} \sim \frac{U_J/(z/D)}{z} = \left(\frac{U_J}{D}\right)/(z/D)^2 \propto U_J/D, \quad (2)$$

where δ_{FWHM} is the jet full-width at half maximum defined from the velocity profile, z is the vertical location within the jet, U_C is the jet centerline velocity, and the effect of virtual origin is intentionally neglected for far-field locations. On the basis of Eq. (2), comparison of extinction tendency among jet flames only requires assessing U_J/D. Preliminary experiments using an existing, crudely-made piloted jet burner with $D = 3.8$ mm suggested that frequent extinction starts to occur at $Re = 30\,000$, which sets the upper limit for U_J/D as $1.8 \times 10^4 \, \mathrm{s}^{-1}$. Figure 2 plots U_J/D for $Re = 15\,000$, 20 000, and 25 000.

Figure 2 indicates the allowed range for the inner tube diameter satisfying all three constraints. For instance, if Re
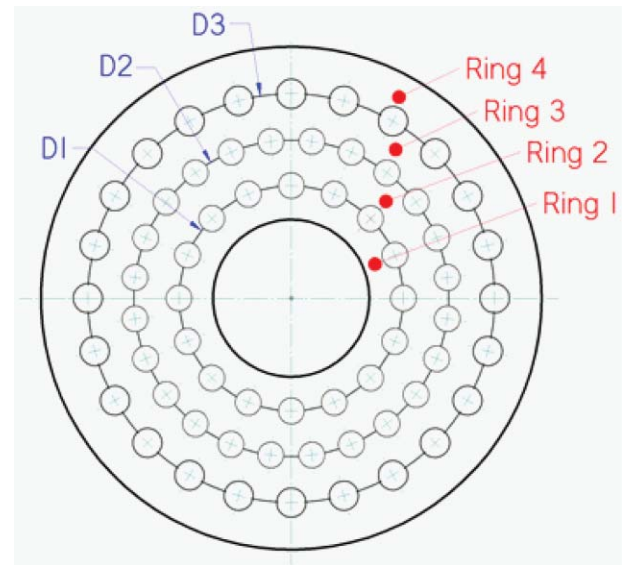

FIG. 3. (Color online) Design diagram for the pilot flame plate, showing the key parameters, whose values are given in Table I.

$= 20\,000$ is the target, the inner jet diameter is limited from 3.1 to 3.8 mm. For our burner, this jet diameter (inner diameter, or ID) was chosen to be 3.2 mm, in order to keep the flame height relatively short. Note that, if a smaller Reynolds number is targeted, such as 15 000, a much wider range of the inner jet diameter is allowed.

A critical aspect of designing laboratory burners for producing data that can be compared to numerical models is to control and/or accurately measure the boundary conditions for the burner so that they are well known and can be suitably modeled.[1] For jet flame burners, the velocity profile of the gas jet at the burner exit plane is a critically important variable. For this reason, for our burner the length of the inner tube is about 540 mm, nearly 170 jet diameters, which assures a fully developed turbulent pipe flow profile at the jet exit.

The outer tube has an ID of 15.2 mm and an OD of 19.1 mm. Situated between the two tubes, the pilot plate has three concentric rows of evenly distributed holes, as shown in Fig. 1(b). The size, number, and spacing between holes are deliberately chosen such that the pilot flames produce a uniform flow rate of flame products across the pilot flame annulus at the burner exit plane. Assuming that the mean reactant gas velocity is the same for all holes, this requirement translates to having uniform porosity (the percentage of hole area) in the four rings, as defined by the circles of hole centers and the two tube walls (Fig. 3). Table I tabulates the dimensions of the pilot plate. Note that the porosities of the innermost and outermost rings (Rings 1 and 4) are smaller than the others, because a greater distance between the holes and corresponding tube walls is required to avoid flame quenching along the walls of the annulus. Such design of the pilot plate using uniform porosity, different from the previous Sydney burner,[5] is believed to be advantageous in creating an evenly distributed temperature boundary. The pilot plate is recessed from the tube lip by 3.2 mm. Figure 1(c) shows the base of a turbulent ethylene flame, with pilot flames appearing as small blue cones surrounding the main jet.

TABLE I. Design specifications of the pilot plates used for the gas- and liquid-fuel burners.

Burner type	D1[a], d1[b], n1[c]	D2, d2, n2	D3, d3, n3	Porosities (Rings 1–4)
Gas-fuel	6.81, 0.79, 16	9.55, 0.79, 24	12.34, 0.89, 24	0.205, 0.276, 0.276, 0.123
Liquid-fuel	6.35, 0.79, 16	9.35, 0.79, 24	12.34, 0.89, 24	0.203, 0.263, 0.260, 0.123

[a]D1 to D3 are diameters of three circles connecting hole centers (in mm).
[b]d1 to d3 are the hole diameters at three rows (in mm).
[c]n1 to n3 are the number of holes at three rows.

The whole burner is constructed from smooth-bore seamless stainless steel 304 tubing. The burner tip is not tapered to a "knife edge," as are some other jet burners.[2,5] This decision not to taper the tubing was made to simplify the attachment of the pilot flame plate, to reduce ambiguities of the actual flow geometry and velocity profile at the burner exit, to keep the burner exit plane relatively sturdy and immune from damage, and to simplify the meshing at the burner exit plane for numerical modeling. Tapering has been argued for on the basis of reducing the generation of vortices during fluid dynamic mixing of parallel flow streams at different velocities and thereby potentially reducing flame stability. In our experience with the current burner design, however, the jet flames were found to be very stable up to high burner jet Reynolds numbers.

B. Liquid fuel combustor

The liquid-fuel burner is designed using a slightly different approach than the gas-fuel burner. To avoid the complications of modeling liquid sprays and droplet evaporation within turbulent spray flames,[56] which is still an active area of research, the fuel is pre-vaporized before being fed into a piloted jet burner to establish a fuel vapor jet flame.

Figure 4 illustrates the fuel delivery system. A high-pressure, diaphragm-type metering pump (m-Roy H, Milton Roy) draws liquid fuel from a tank, and sends it through an open cone diesel spray nozzle (Del-O-Flo A, Delavan) to create a mist of tiny droplets, which subsequently evaporates inside a vaporizer. Design drawings of the vaporizer are shown in Fig. 5. The vaporizer consists of an aluminum tubular heat exchanger with radial fins inside and two adjacent clamp-on band heaters (THERMASLEEVE, Watlow) outside. Complete fuel vaporization is assured by maintaining the vaporizer at a temperature above the boiling points of all fuel components. The fuel vapor is then carried to the piloted jet burner
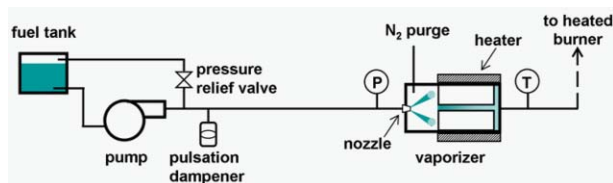

FIG. 4. (Color online) Schematic of the fuel delivery system for the liquid-fuel burner. Liquid fuel is pre-vaporized before entering the combustor. "P" and "T" stand for pressure and temperature sensors, respectively.
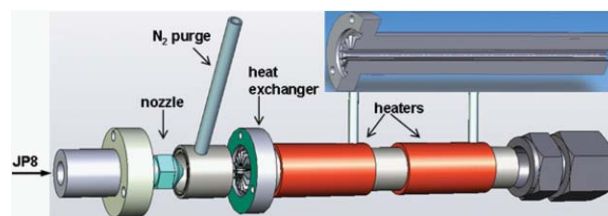

FIG. 5. (Color online) 3D model of the liquid fuel vaporizer. The insert on the top right shows the sectional view of the externally heated, finned heat exchanger.

through a flexible hose. The hose, the burner fuel tube, and all fittings are electrically heated to prevent any condensation of the fuel vapor.

This vapor production scheme offers several advantages, as compared to direct boiling or using a heated porous plug. First, fine atomization of fuel followed by immediate evaporation avoids differential evaporation of fuel components with disparate boiling points (i.e., fuel distillation), as typically occurs in direct boiling vaporizers. For instance, for the JP-8 surrogate used in our study, the two components, m-xylene and n-dodecane, have boiling points of 139 °C and 216 °C, respectively. During experiments, the heaters, whose output is controlled by temperature controllers (I series, OMEGA Engineering), maintain the vaporizer at 300 °C in order to flash vaporize both fuel components. An analysis of the re-condensed vapor using a mass spectrometer verified that the vapor composition is unchanged from its liquid form and also indicated there was no thermal decomposition of the fuel components at this temperature. Second, the fuel flow rate can be conveniently controlled. For a given nozzle geometry, the flow rate through the nozzle solely depends on the supply pressure. Therefore, the vapor flow rate can be changed by modifying the pump output pressure, as long as the heating power of electric heaters can provide sufficient heating. Calibration of the vapor flow rate is performed by routing the generated vapor through a water-cooled Graham condenser and measuring the condensed liquid volume at room temperature. This calibration method has an estimated uncertainty of 1%.

Since fuel flow rate is related to the pump output pressure, steady operation of the burner requires that fluctuations in pump pressure be minimized. This is achieved by installing a pulsation dampener (Sentry, Blacoh Fluid Control) just downstream of the pump (Fig. 4). Monitored by a pressure transducer (100 series, TESCOM), the nozzle atomization pressure is stabilized within 1%, which results in less than 1% variation in the fuel supply rate for a given operational setpoint.

The liquid fuel jet burner is designed using a similar concept as its gas-fuel counterpart, except that an electric cable heater coils around the inner fuel tube to maintain the fuel vapor above its condensation point. Sizing of the inner tube follows the same procedure as in the gas-fuel burner. Flame height calculations using Eq. (1) are shown in Fig. 6 for $Re = 15\,000$, $20\,000$ and $25\,000$ with the JP-8 surrogate. Note that flames burning aromatic-containing fuels such as the JP-8 surrogate are strongly sooting and hence radiating. For Fr_f less than 2, which is the case for most examined
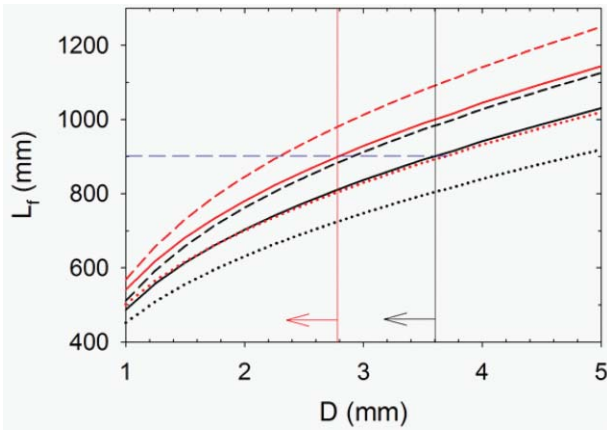
FIG. 6. (Color online) Estimated flame height for JP-8 surrogate vapor (at 300 °C) as a function of fuel jet diameter. Estimates are shown for both negligible radiation heat loss and 40% radiation loss (higher sequence of curves). The flame height is required to be less than 900 mm. Three Reynolds numbers are drawn: 20 000 (solid), 15 000 (dotted), and 25 000 (dash). The vertical lines together with arrows indicate the allowable range of fuel jet diameter.

conditions, the impact of radiation heat loss on flame length can be approximated as[54,55]

$$L_f \propto Fr_f^{2/5} \propto \Delta T_f^{-1/5} \quad \text{when} \quad Fr_f \le 2, \tag{3}$$

where ΔT_f is the characteristic temperature rise due to combustion and can be taken as the temperature difference between a flame and its environment,

$$\Delta T_f = \Delta T_{f,ad}(X_C - X_R), \tag{4}$$

where $\Delta T_{f,ad}$ is the adiabatic flame temperature rise, and X_C and X_R are the combustion efficiency (nearly equal to 1) and radiant fraction, respectively. According to Eqs. (3) and (4), a radiant fraction of 40%, as estimated for JP-8 flames, would lead to an 11% increase in flame length (Fig. 6). Therefore, an acceptable maximum flame length of 900 mm sets the upper bound for the inner tube ID as 2.8 mm for a target *Re* of 20 000.

In estimating flame height and Reynolds number, the density and viscosity of the fuel vapor are needed. Since these properties for our JP-8 surrogate are not available in the literature, their calculations deserve a few notes. As the vapor temperature at the jet exit is at least 80 °C above the boiling point of each constituent, the vapor is expected to behave close to an ideal gas. Hence, the density of the JP-8 vapor mixture is assumed to follow the ideal gas law,

$$\rho = P \cdot MW_{mix}/(RT), \tag{5}$$

where P is the pressure, T is the temperature, R is the universal gas constant, and MW_{mix} is the molecular weight of the mixture. The viscosity of this two-component mixture is calculated from the well-known Wilke's relation,[57]

$$\mu_{mix} = \frac{\mu_1}{1 + (x_2/x_1)\phi_{12}} + \frac{\mu_2}{(1 + x_1/x_2)\phi_{21}}, \tag{6}$$

where μ_i is the viscosity of component i, x_i is the corresponding mole fraction, and the dimensionless constant ϕ_{ij} is de-

TABLE II. Properties of *m*-xylene, *n*-dodecane, and the JP-8 surrogate.

Species	Liquid volume fraction (A:B)	Mole fraction (A:B)	MW (g/mol)	ρ at 300 °C (kg/m³)	μ at 300 °C (10^{-7} kg/m s)
m-xylene (A)			106.2	2.258	120.1
n-dodecane (B)			170.3	3.622	88.58
JP-8	0.23:0.77	0.356:0.644	147.5	3.136	147.5

fined as

$$\phi_{ij} = \frac{[1 + (\mu_i/\mu_j)^{1/2}(MW_j/MW_i)^{1/4}]^2}{(2\sqrt{2})[1 + (MW_i/MW_j)]^{1/2}}, \tag{7}$$

where $i = 1,2$ indicate *m*-xylene and *n*-dodecane, respectively, with properties taken from Ref. 58. Table II tabulates the calculated properties.

Assessment of the strain-rate requirement would put a lower bound on the inner tube ID, as previously explained for the gas-fuel burner. However, as there was no available data to establish the criterion for frequent extinctions of the JP-8 surrogate jet flames before the burner was built, this lower tube diameter bound could not be estimated. Knowing that for a given Reynolds number a smaller jet diameter produces higher U_J/D and hence more extinction-prone flames, we chose 2.5 mm for the ID of the inner jet. The corresponding OD and burner length are 4.0 mm and 538 mm, respectively.

The outer tube has the identical dimensions as for the gas-fuel burner. The pilot plate is designed along the same principle as for the gas-fuel burner and has the specifications listed in Table I.

C. Choice of flames and operating conditions

During experiments, the jet burners are mounted on top of a vertical wind tunnel that provides uniform co-flowing air at a low velocity (Fig. 1(c)). The coflow screens out disturbances from room ventilation and establishes a consistent boundary condition for matching experiments with models. The whole burner assembly is mounted on a motorized, 3-axis traverse system, which moves the burner relative to fixed laser beam positions to change the measurement location.

Five flames were identified as canonical flames for detailed experimental investigations, as shown in Table III. The four ethylene jet flames have fuel jet *Re* ranging from 10 000 to 25 000, thus allowing an investigation of the effects of different levels of turbulence. It should be mentioned that the gas-fuel burner can support stable attached ethylene flames with *Re* well above 30 000, where frequent extinctions occur, thereby possessing the potential of investigating strong turbulence-chemistry interactions. The one JP-8 flame established on the liquid-fuel burner burns vaporized JP-8 surrogate with a *Re* of 20 000. For all these flames, the pilot flames are fueled by premixed ethylene and air with an equivalence ratio of 0.9. The flow rate of the pilot mixture corresponds to

TABLE III. Flow parameters of the flames used in our experiments.

Fuel	Re	Q^a (kW)	Fr_f^b	$L_{f,e}^c$ (mm)	$L_{f,m}^d$ (mm)	FR_f^e (slpm)	FR_p^f (slpm)	U_∞^g (m/s)	T_f^h (°C)	T_p^i (°C)
C2H4	10 000	12.0	1.0	652	730	13.2	4.45	0.60	21	21
	15 000	18.0	1.4	755	775	19.8	6.68			
	20 000	24.0	1.9	832	830	26.4	8.91			
	25 000	30.0	2.4	890	861	33.0	11.14			
JP-8	20 000	16.5	1.0	860	872	0.0295	6.09	0.67	300	205

[a] Heating value of the main fuel jet.
[b] Froude number of flame; for JP-8, assumes 40% radiation loss.
[c] Estimated visible flame length; for JP-8, assumes 40% radiation loss.
[d] Measured visible flame length.
[e] Volumetric flow rate of main fuel jet (liquid flow for JP-8).
[f] Volumetric flow rate of pilot flame premixture.
[g] Velocity of coflow air.
[h] Temperature of unburnt fuel.
[i] Temperature of pilot flame premixture.

2% of the heat release rate of the main fuel jet. Detailed flow parameters are listed in Table III. Note that these flames with Fr_f ranging between 1.0 and 2.4 fall in the transitional regime, where both buoyancy and jet momentum are important.[54] Visible flame heights estimated from Eq. (1) generally match measured values well, confirming the validity of using this relation.

III. PRELIMINARY CHARACTERIZATION

The open flame configuration permits convenient access for both optical and probe-based measurements. The five canonical flames were characterized with qualitative methods, including direct photography, OH LIF planar imaging and soot LII planar imaging. In addition, measurements of the burner lip temperature boundary with line Rayleigh imaging are presented for ethylene flames. Much can be learned from these preliminary measurements, such as the flame size, the frequency of occurrence of local extinction, and soot behavior.

A. Visual observation

In general, a sooty jet flame has a blue soot-free region near the nozzle (Fig. 1(c)) followed by a soot-laden region downstream. Soot produced in the flame is either consumed or escapes from the flame as smoke. The length of the soot-free region depends on the fuel, the fuel jet diameter, and the fuel jet velocity. Figure 7 presents fast-shutter photos of the four ethylene jet flames. With the 1/1600 s exposure time, the soot-free region is nearly invisible and the sooty regions appear orange, from the broad-band soot radiation. An increase in jet velocity pushes the sooty edge (the bottom edge of the soot-containing region) downstream. The photographs of the flames also show a progression in flame wrinkling with increasing jet Re. The flame with a Reynolds number of 10 000 shows smooth, large-scale vortex rollup, particularly as the distance from the nozzle increases (and buoyancy effects become relatively stronger). For flames with higher Re, the luminous flame front shows more intense wrinkling and smaller characteristic flame structures, reflecting a more turbulent flow field. The flame also broadens radially with the increase in Re, reflecting the increased rate of mixing between the fuel jet and the air coflow.

Since the JP-8 flame uses a burner with a smaller fuel tube diameter than the ethylene flames, there is limited value in comparing these flames. Instead, we can compare the JP-8 flame to an ethylene flame established on the same (liquid-fuel) burner with the same fuel jet Re (20 000). As shown in Fig. 8, these two flames look somewhat different. While the ethylene jet flame has a fairly long blue, soot-free region near the nozzle, the JP-8 flame is almost completely devoid of

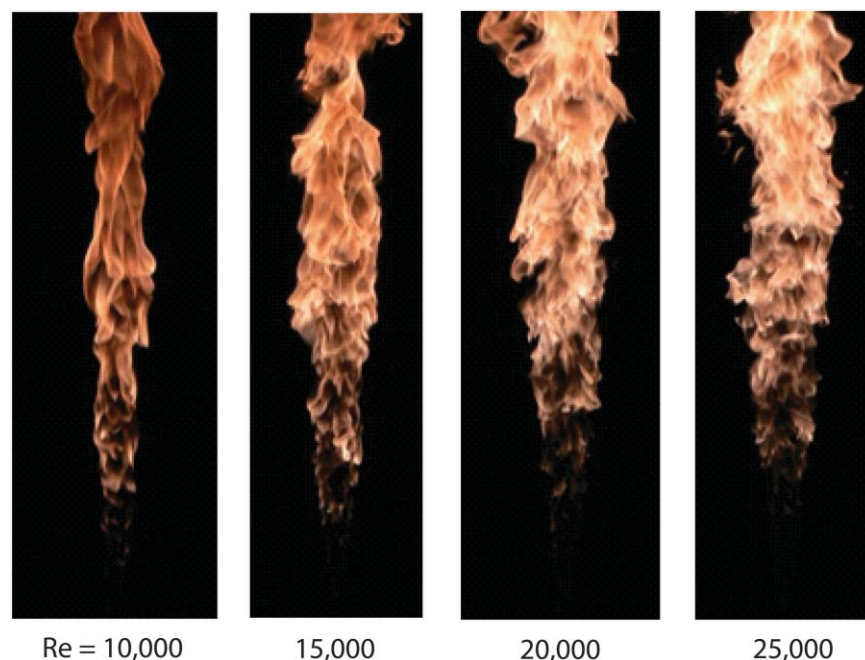Re = 10,000   15,000   20,000   25,000

FIG. 7. (Color online) Fast-shutter (1/1600 s) photographs of four ethylene jet flames with the indicated fuel jet Reynolds numbers.
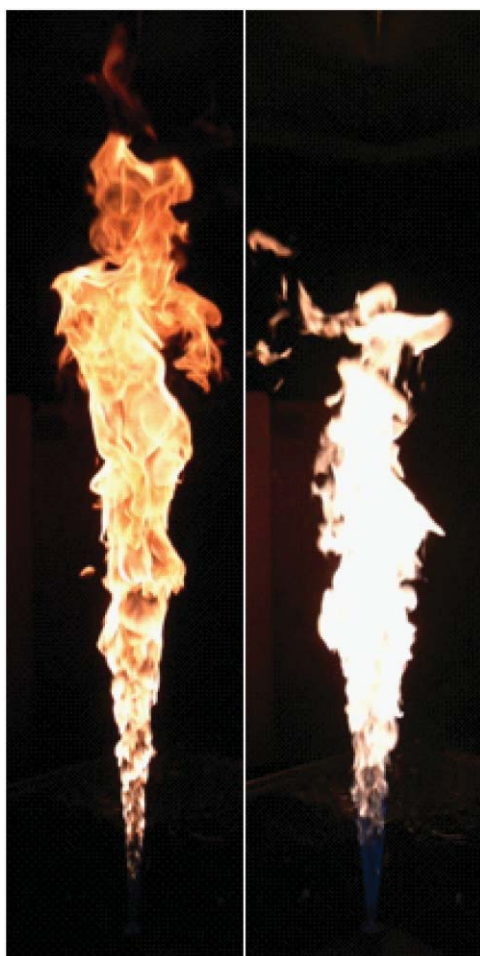
FIG. 8. (Color online) Fast-shutter photographs of a JP-8 flame (left column) and an ethylene jet flame (right column), anchored on the same liquid-fuel burner. The ethylene is not preheated before combustion. The shutter speed is 1/1000 s, and both flames have a Reynolds number of 20 000.

this region. Furthermore, the JP-8 flame photograph shows a consistent orange glow, in contrast to the bright, white sooty region of the ethylene flame. Direct visual observation of the two flames revealed the same general trend, but not nearly as pronounced as suggested in the photographs in Fig. 8. Therefore, we believe the actual difference in flame color was exaggerated by the use of an automatic aperture setting in taking the photographs. In part, the difference in flame color reflects different characteristic soot temperatures within the flames. The JP-8 flame, because it forms soot earlier and at higher concentrations, has more radiation heat loss, resulting in lower soot temperatures. It should also be pointed that, while the ethylene flame appears to be nearly non-smoking, a significant amount of smoke is observed to be emitted from the JP-8 flame.

B. Temperature boundary

The burner exit plane temperature boundary condition was measured with line Rayleigh imaging. To perform these measurements, a 532 nm frequency-doubled YAG laser beam was passed 5 mm above the burner lip (to minimize laser scattering interference off of the burner surface) and the resultant
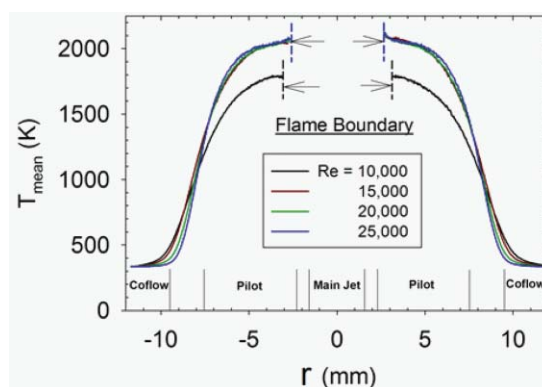

FIG. 9. (Color online) Temperature field at 5 mm downstream from the burner lip measured with line Rayleigh imaging for four piloted ethylene jet flames. The vertical lines at the figure bottom identify dimension of the jet lip.

Rayleigh signal was collected by a CCD camera (PIXIS, Princeton Instruments). At constant pressure, the Rayleigh signal (S_{Ray}) can be converted to temperature (T) according to

$$T = C\sigma/S_{Ray}, \tag{8}$$

where C is the calibration constant and σ is the Rayleigh cross section of the local gas mixture. For general application to flames, the use of Rayleigh scattering to determine T requires simultaneous knowledge of the Rayleigh cross section of the local gas mixture, which often calls for combined Rayleigh-Raman-LIF measurements with a sophisticated setup and cannot be applied to flame regions containing soot or PAH.[4] Fortunately, the Rayleigh cross section of the equilibrium products of the pilot flame mixture (σ_{pilot}) is found to be close to that of air (σ_{air}),

$$\sigma_{pilot} = 1.14\sigma_{air}. \tag{9}$$

Thus, by assuming a uniform Rayleigh cross section outside the flame boundary with the value of σ_{pilot}, we calculated the temperature profile outside the flame boundary, as shown in Fig. 9. Note that, according to Eqs. (8) and (9), such a simplifying assumption leads to no more than 14% overprediction of temperature near the outer edge of the pilot flame annulus, where the gas composition is expected to be dominated by air. The flame boundary mentioned above is determined as the location with the weakest signal, according to Eq. (8) (i.e., for a given Rayleigh cross section the Rayleigh signal is inversely proportional to temperature).

As shown in Fig. 9, the pilot burner successfully produces a flat temperature boundary (and therefore presumably a flat velocity profile) for all of the different pilot flow rates corresponding to different ethylene flames (recall that the pilot flow rate is set to correspond to 2% of the heat release of the main jet). In particular, all the flames except $Re = 10\,000$ have a similar temperature profile outside the flame boundary. The anomalous profile for $Re = 10\,000$ probably results from the inaccurate operation of a mass flow controller for the pilot flame, because the pilot flow rate for this condition was near the lower limit of the flow controller. The temperature profile within the flame boundary could not be deduced from the Rayleigh scattering signals because of uncertainties over the
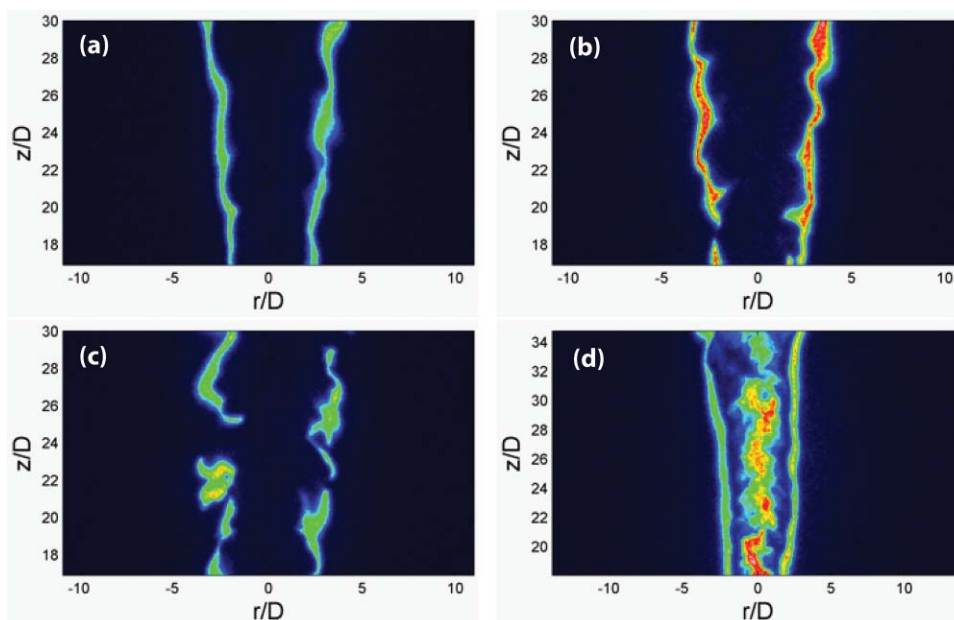
FIG. 10. (Color online) Instantaneous false-color OH PLIF images of three turbulent ethylene jet flames (a, $Re = 15\,000$; b, $Re = 20\,000$; c, $Re = 25\,000$) and one JP-8 flame (d, $Re = 20\,000$). The same intensity map was used to process all of the OH PLIF images.

local Rayleigh scattering cross section of the chemical species mix in this region.

A similar measurement of the temperature boundary was not performed for the JP-8 flame, but the nearly identical design of the pilot plate for this burner as for the gas burner is expected to give equivalent temperature profiles at the burner exit plane.

C. OH LIF imaging

As OH is an important flame marker, planar imaging of OH is an effective method of capturing extinction events, which appear as breaks within otherwise continuous OH layers. To perform these measurements, a UV laser beam at 283.55 nm was generated from the frequency doubled output of a YAG-pumped dye laser. The beam was shaped into a laser sheet with sheet-forming optics and subsequently intersected the flame on an axial plane, exciting OH radicals. The OH fluorescence was detected by an intensified CCD camera (ICCD-MAX, Princeton Instruments) operating with a 100 ns exposure time using a 105-mm focal length, f/4.5 UV Nikkor lens and a band-pass filter set that transmits 304–320 nm. This OH detection scheme provides good discrimination against flame emission, laser scattering and fluorescence from polycyclic aromatics, but accepts fluorescence from single and double-ring aromatics.[59]

Figure 10 shows false-color OH LIF images centered about 24 jet diameters downstream, where strong strain coupled with diminishing influence of the pilot flame results in the highest probability of local flame extinction. For ethylene flames with a Reynolds number of 15 000 or less, breakup of OH layers rarely occurs (Fig. 10(a)). Breaks in the OH layers are occasionally apparent in the ethylene flame with a Re of 20 000 (Fig. 10(b)), and become a frequent feature when the flame Re reaches 25 000 and above (Fig. 10(c)), suggesting

frequent local extinction followed by reignition downstream. Flames remain attached to the burner lip until the fuel jet Re is increased beyond 35 000, when extinction becomes so severe that the flame is partially attached or lifted off from the burner. Clearly, this relationship between the flame Reynolds number and extinction frequency is consistent with our prediction based on U_J / D as shown in Fig. 2. It is also noted that, with the increase in Re, the OH layers at this height change from smooth sheets (Fig. 8(a)) to rugged and kinked structures (Figs. 10(b) and 10(c)), indicating the enhanced interactions between turbulence and the flame zone.

Figure 10(d) shows an OH fluorescence image of the JP-8 flame over a similar range of near-burner heights as for the ethylene flame images. Note that the strong fluorescence around the jet axis (r/D = 0) is due to small-ring aromatics, probably dominated by the m-xylene that is in the fuel vapor. The OH layer along the sides of the jet axis appears smooth and seldom broken, and behaves more like that in the ethylene jet flame with a Re of 15 000 than that with a Re of 20 000. The fact that this JP-8 flame does not exhibit local extinctions even for a Re of 20 000 justifies our choice of the inner tube ID in Sec. II.

D. Soot LII imaging

Soot is detected with LII[60, 61] using an infrared laser sheet at 1064 nm generated from the fundamental output of a pulsed Nd:YAG laser. The laser sheet passes through the jet axis and momentarily heats the soot particles to their evaporation temperature (>4000 K). The resultant thermal radiation from heated soot particles, when collected with an ICCD camera (PI-MAX, Princeton Instruments) and short exposure time (50 ns), dwarfs flame chemiluminescence and indicates the location of soot layers. While the quantitative measurement
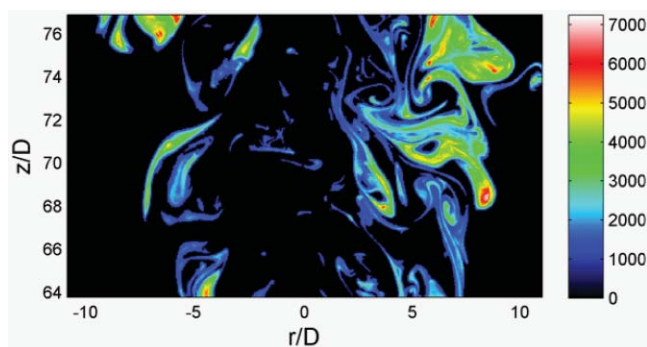
FIG. 11. (Color online) Instantaneous false-color soot LII image at mid-height of the turbulent ethylene jet flame with $Re = 20\,000$. The same color scale is used as in Fig. 10.

of soot concentration is possible with this technique, it is beyond the scope of this paper.

Although soot forms earlier and has greater concentrations in the JP-8 flame as compared to the four ethylene flames, images of soot-containing regions in these flames are qualitatively similar. Figure 11 shows a sample snapshot of soot in the ethylene flame with a Re of 20 000. Evidently, soot is present in multiple discrete layers within the flame sheet, in sharp contrast to the OH, which is present in a single outer layer at the flame sheet in the same flame. Sooty structures show vortex-like curvature, because of the small diffusivity of soot and its persistent nature, until passing into an active oxidation zone.[62]

Both quantitative measurements of soot concentrations and particle size and qualitative measurements of soot layer characteristics in these flames (as shown in Fig. 11) can, together with the measurement of other flame parameters, provide important data for the development and validation of turbulent non-premixed flame models for sooting fuels. The initial measurements reported in this paper show that the burner designs that have been developed for this purpose can successfully produce the requisite flame stability and well-known boundary conditions required for accurate modeling of such flame systems.

IV. CONCLUSIONS

In this paper, we report on the design of two non-premixed jet burners for establishing robust turbulent flames for hydrocarbon fuels of C_{2+}, one using gaseous fuel and the other using higher-C liquid fuel. Both burners use coannular pilot flames to stabilize the main flame, even at high jet velocities. Supplied with ethylene, the gas-fuel burner can support stable, attached flames with a fuel jet Reynolds number surpassing 30 000. The liquid-fuel burner pre-vaporizes the fuel before combustion and has been successfully demonstrated for a JP-8 surrogate.

Four ethylene jet flames and one JP-8 flame were chosen as canonical flames for experimental investigation. It is found that the flame length of these piloted jet flames can be satisfactorily predicted by a correlation previously developed for simple jet flames, when radiation loss is properly accounted for. The burner exit plane temperature profile was measured for

the four ethylene flames using line Rayleigh imaging. Imaging of OH suggests the ethylene flame does not experience significant local extinctions until the flame Reynolds number reaches 25 000, and the JP-8 flame with a Re of 20 000 behaves similarly to ethylene jet flames with lower Re. Soot in all the flames is qualitatively similar and is present as multiple curved layers within the boundary of the flame sheet.

These two burners hold great promise as model combustors for studying the non-premixed combustion of C_{2+} hydrocarbon fuels in turbulent environments. Their open configuration provides easy access for experimental measurements, particularly, optical diagnostics. Their simple geometry, well-defined boundary conditions, and single-phase characteristic all lend convenience to numerical modeling.

[1]R. S. Barlow, Proc. Combust. Inst. **31**, 49 (2007).
[2]W. Meier, S. Prucker, M. H. Cao, and W. Stricker, Combust. Sci. Technol. **118**, 293 (1996).
[3]V. Bergmann, W. Meier, D. Wolff, and W. Stricker, Appl. Phys. B **66**, 489 (1998).
[4]R. S. Barlow, G. J. Fiechtner, C. D. Carter, and J. Y. Chen, Combust. Flame **120**, 549 (2000).
[5]A. R. Masri, R. W. Dibble, and R. S. Barlow, Prog. Energy Combust. Sci. **22**, 307 (1996).
[6]J. H. Frank and R. S. Barlow, Proc. Combust. Inst. **27**, 759 (1998).
[7]R. S. Barlow and J. H. Frank, Proc. Combust. Inst. **27**, 1087 (1998).
[8]R. S. Barlow, A. N. Karpetis, J. H. Frank, and J. Y. Chen, Combust. Flame **127**, 2102 (2001).
[9]R. S. Barlow, J. H. Frank, A. N. Karpetis, and J. Y. Chen, Combust. Flame **143**, 433 (2005).
[10]W. P. Jones and V. N. Prasad, Combust. Flame **157**, 1621 (2010).
[11]H. Pitsch and H. Steiner, Phys. Fluids **12**, 2541 (2000).
[12]M. R. H. Sheikhi, T. G. Drozda, P. Givi, F. A. Jaberi, and S. B. Pope, Proc. Combust. Inst. **30**, 549 (2005).
[13]T. W. J. Peeters, P. P. J. Stroomer, J. E. de Vries, D. J. E. M. Roekaerts, and C. J. Hoogendoorn, Proc. Combust. Inst. **25**, 1241 (1994).
[14]A. R. Masri and R. W. Bilger, Proc. Combust. Inst. **20**, 319 (1985).
[15]T. Landenfeld, A. Kremer, E. P. Hassel, J. Janicka, T. Schäfer, J. Kazenwadel, C. Schulz, and J. Wolfrum, Proc. Combust. Inst. **27**, 1023 (1998).
[16]B. F. Magnussen, Proc. Combust. Inst. **15**, 1415 (1975).
[17]B. F. Magnussen, B. H. Hjertager, J. G. Olsen, and D. Bhaduri, Proc. Combust. Inst. **17**, 1383 (1979).
[18]H. A. Becker and S. Yamazaki, Proc. Combust. Inst. **16**, 681 (1977).
[19]H. A. Becker and D. Liang, Combust. Flame **32**, 115 (1978).
[20]H. A. Becker and S. Yamazaki, Combust. Flame **33**, 123 (1978).
[21]H. A. Becker and D. Liang, Combust. Flame **44**, 305 (1982).
[22]O. Nishida and S. Mukohara, Combust. Flame **47**, 269 (1982).
[23]J. H. Kent and S. K. Bastin, Combust. Flame **56**, 29 (1984).
[24]J. H. Kent and D. Honnery, Combust. Sci. Technol. **54**, 383 (1987).
[25]S. M. Jeng and G. M. Faeth, J. Heat Trans. **106**, 891 (1984).

[26]J. P. Gore and G. M. Faeth, Proc. Combust. Inst. **21**, 1521 (1986).

[27]J. P. Gore and G. M. Faeth, J. Heat Transfer **110**, 173 (1988).

[28]Y. R. Sivathanu, J. P. Gore, and J. Dolinar, Combust. Sci. Technol. **76**, 45 (1991).

[29]Y. Zheng and J. P. Gore, Proc. Combust. Inst. **30**, 727 (2005).

[30]W. L. Flower, Proc. Combust. Inst. **22**, 425 (1988).

[31]S. R. Turns, J. A. Lovett, and H. J. Sommer III, Combust. Flame **77**, 405 (1989).

[32]S. R. Turns and J. A. Lovett, Combust. Sci. Technol. **66**, 233 (1989).

[33]S. R. Turns and F. H. Myhr, Combust. Flame **87**, 319 (1991).

[34]S. R. Turns and R. V. Bandaru, Combust. Flame **94**, 462 (1993).

[35]S. Y. Lee, S. R. Turns, and R. J. Santoro, Combust. Flame **156**, 2264 (2009).

[36]K. J. Young, C. D. Stewart, and K. J. Syed, in *Proceeding of Tenth International Symposium on Air Breathing Engines (ISABE) Meeting* (AIAA, Virginia, 1991), p. 239.

[37]K. J. Young, C. D. Stewart, and J. B. Moss, Proc. Combust. Inst. **25**, 609 (1994).

[38]B. Hu, B. Yang, and U. O. Koylu, Combust. Flame **134**, 93 (2003).

[39]B. Yang and U. O. Koylu, Combust. Flame **141**, 55 (2005).

[40]G. M. Faeth and G. S. Samuelsen, Prog. Energy Combust. Sci. **12**, 305 (1986).

[41]M. Köhler, K. P. Geigle, W. Meier, B. M. Crosland, K. A. Thomson, and G. J. Smallwood, "Sooting turbulent jet flame: characterization and quantitative soot measurements," Appl. Phys. B (in press).

[42]S. Navarro-Martinez and A. Kronenburg, Proc. Combust. Inst. **32**, 1509 (2009).

[43]I. Glassman, J. Proc. Combust. Inst. **22**, 295 (1988).

[44]A. C. Eckbreth, J. Appl. Phys. **48**(11), 4473 (1977).

[45]A. D'Alessio, A. D'Anna, G. Gambi, and P. Minutolo, J. Aerosol Sci. **29**(4), 397 (1998).

[46]I. M. Aksit and J. B. Moss, Combust. Flame **145**, 231 (2006).

[47]M. E. Mueller, G. Blanquart, and H. Pitsch, Combust. Flame **156**, 1143 (2009).

[48]J. S. Bhatt and R. P. Lindstedt, Proc. Combust. Inst. **32**, 713 (2009).

[49]T. Chittipotula, G. Janiga, and D. Thévenin, Proc. Combust. Inst. **33**, 559 (2011).

[50]M. Ihme and H. Pitsch, Combust. Flame **155**, 90 (2008).

[51]V. Sankaran, T. G. Drozda, and J. C. Oefelein, Proc. Combust. Inst. **32**, 1571 (2009).

[52]B. A. Sen, E. R. Hawkes, and S. Menon, Combust. Flame **157**, 566 (2010).

[53]M. B. Colket, personal communication (December 2008).

[54]M. A. Delichatsios, Combust. Flame **92**, 349 (1993).

[55]S. R. Turns, *An Introduction to Combustion: Concepts and Applications* (McGraw-Hill, Boston, 2000).

[56]H.-W. Ge, I. Düwel, H. Kronemayer, R. W. Dibble, E. Gutheil, C. Shulz, J. Wolfrum, Combust Sci. Technol. **180**, 1529 (2008).

[57]C. R. Wilke, J. Chem. Phys. **18**, 517 (1950).

[58]*Physical and Thermodynamic Properties of Pure Compounds: Data Compilation*, edited by T. E. Daubert and R. P. Danner (Taylor and Francis, Washington DC, 1998).

[59]G. Zizak, Altas of Fluorescence Spectra of Aromatic Hydrocarbons (Vol. 1), http://www.tempe.mi.cnr.it/zizak/atlas/cld-atlas-eng.htm.

[60]R. J. Santoro and C. R. Shaddix, "Laser-Induced Incandescence," in *Applied Combustion Diagnostics*, edited by K. Kohse-Höinghaus and J. B. Jeffries (Taylor and Francis, New York, 2002).

[61]C. Schulz, B. F. Kock, M. Hofmann, H. Michelsen, S. Will, B. Bougie, R. Suntz, and G. Smallwood, Appl. Phys. B **83**, 333 (2006).

[62]W. M. Roquemore, V. Katta, S. Stouffer, V. Belovich, R. Pawlik, M. Arstingstall, G. Justinger, J. Gord, A. Lynch, J. Zelina, and S. Roy, Proc. Combust. Inst. **32**, 729 (2009).